8. D. Svintsov, V. Vyurkov, V. Ryzhii, and T. Otsuji, Voltage-controlled surface plasmon-polaritons in double graphene layer structures, J Appl Phys 113 (2013), 053701.
9. M. Tamagnone, J.S. Gómez-Díaz, J.R. Mosig, and J. Perruisseau-Carrier, Reconfigurable terahertz plasmonic antenna concept using a graphene stack, Appl Phys Lett 101 (2012), 214102.
10. R. Filter, M. Farhat, M. Steglich, R. Alaee, C. Rockstuhl, and F. Lederer, Tunable graphene antennas for selective enhancement of THz-emission, Opt Express 21 (2013), 3737–3745.
11. J.S. Gómez-Díaz and J. Perruisseau-Carrier, Graphene-based plasmonic switches at near infrared frequencies, Opt Express 21 (2013), 15490–15504.
12. M. Liu, X. Yin, and X. Zhang, Double-layer graphene optical modulator, Nano Lett 12 (2012), 1482–1485.
13. R.E. Collin, Field theory of guided waves, McGraw-Hill Book Co., New York, 1960.
14. D. Lioubtchenko, S. Tretyakov, and S. Dudorov, Millimeter-wave waveguides, Kluwer Academic Publishers, Boston, MA, 2003.

METHOD TO SENSITIZE AN ARC-INDUCED LPFG-BASED SENSOR USING DOUBLE-PASS CONFIGURATION

Mey C. Loh,[1] Faidz A. Rahman,[1] Hideki Kuramitz,[2] and Yun T. Yong[3]
[1] Faculty of Engineering and Science, Universiti Tunku Abdul Rahman, Kuala Lumpur, Malaysia; Corresponding author: faidzar@utar.edu.my
[2] Department of Environmental Biology and Chemistry, Graduate School of Science and Engineering for Research, University of Toyama, Gofuku, Japan
[3] Faculty of Engineering and Green Technology, Universiti Tunku Abdul Rahman, Kampar, Malaysia

Received 25 April 2014

ABSTRACT: *The sensitivity of the arc-induced long period fiber grating (LPFG) sensor was improved utilizing the double-pass configuration. The sensitivity in terms of transmission attenuation of the resonance wavelength for the double-pass LPFG configuration was better compared to the single-pass configuration when it was used to monitor the avidin–biotin interaction over a period of 60 min.* © 2014 Wiley Periodicals, Inc. Microwave Opt Technol Lett 56:2766–2769, 2014; View this article online at wileyonlinelibrary.com. DOI 10.1002/mop.28701

Key words: *long period fiber grating; double-pass configuration; optical fiber sensor; avidin–biotin interaction; biosensor*

1. INTRODUCTION

Long period fiber gratings (LPFGs) have been known for more than 10 years [1]. LPFGs are structures with periodic modulations of the refractive index along the length of a fiber where under certain phase-matching conditions, the fundamental core mode couples to the discrete cladding modes. Spectrally selective loss can be obtained due to the wavelength dependence of the coupling from the guided mode to the cladding modes. Usually, LPFGs are written by lasers with spectral range from ultraviolet to far infrared [2]. LPFGs can also be written with an electric arc [3] which uses electric arc discharges. The electric arc method is mostly favored for its simplicity, low cost, flexibility, and applicability. Some of the advantages of arc-induced gratings include resistance to thermal annealing, and does not require preprocessing which is time consuming. The LPFG transmission characteristics can be sensitized via numerous methods based the turning points of the dispersion mode of the LPFG [4], etching of the cladding [5], using doped fibers for LPFG fabrication [6], and layer-by-layer of polyelectrolytes or silanization [7].

In work related to erbium doped fiber amplifier (EDFA), double-pass was proposed to achieve high gain, low noise figure and improved flat gain with a gain variation of less than 1 dB over 33 nm [8]. To address increasing demand for greater bandwidth in telecommunication systems, Harun and Ahmad proposed a double-pass L-band EDFA which uses an optical circulator to double-pass the signal that kept the noise figure low while having significant gain improvement [9]. By utilizing fiber grating (FBG) and double-pass method, Tsair-Chun Liang managed to implement an L-band EDFA of high clamped gain and low noise figure for DWDM systems [10].

Adapting the idea from the work done on EDFAs, we are proposing the use of double-pass configuration to increase the transmission attenuation of the LPFG resonance wavelength and subsequently improve the sensitivity of the LPFG when used as an optical sensor. Due to the longer path in which the light passes through the grating region in the double-pass configuration, there will be better coupling between the core and cladding modes thus giving better transmission attenuation and sensitivity toward changes to the surrounding environment. To our knowledge, there are no known researches on double-pass arc-induced LPFG configuration as optical sensors.

For the purpose of confirming sensitivity of the double-pass LPFG configuration, the sensor was used to monitor the avidin–biotin interaction over a period of time. This avidin–biotin interaction has diverse applications in various analytical fields especially for molecular detection. The avidin family of proteins, with 4 biotin-binding sites per molecule, is capable of forming tight complexes with biotinylated compounds [11]. Biotin is also known as vitamin H (cis-hexahydro-2-oxo-1-H-thieno-[3,4]-imidazoline-4-valeric acid) and can form an avidin–-biotin complex that is very stable. Interaction between avidin and biotin is rapid and it is used for in situ attachment of labels for numerous applications. Some examples are label-free optical sensors [12] and chip-based capillary electrophoretic method for avidin determination [13]. The affinity of avidin–biotin complex is high and the avidin–biotin bond is the strongest known biological interaction between a ligand and a protein (dissociation constant of 10–15 M) [14]. The interaction of the avidin–biotin on the grating surface changes the effective index of the cladding thus affecting the respond of the light passing through the LPFG.

2. EXPERIMENTAL DETAILS

SMF28 fibers were used where the fiber coating was stripped off before the gratings were formed on the fiber. The LPFG with grating period of 675 μm and grating length of about 23.6 mm was fabricated using high voltage arc and transmission spectrum formed was observed using an optical spectrum analyzer. After the LPFG fabrication, the grating region of the optical fiber was coated with gold nanoparticles (GNP) synthesized via Frens method [15], that is, utilizing electrostatic self-assembly for 1 h. After coating of GNP, the optical fiber was rinsed with deionized water and left to dry in air before the immobilization of avidin. Avidin monolayer was immobilized on the GNP surface using the self-assembly method before it was used to monitor the biotin interaction. Avidin coated LPFG was prepared by immersing the GNP modified LPFG sensor in a phosphate buffer solution (PBS) with pH 7.5 and containing 10 μM of avidin for 60 min.

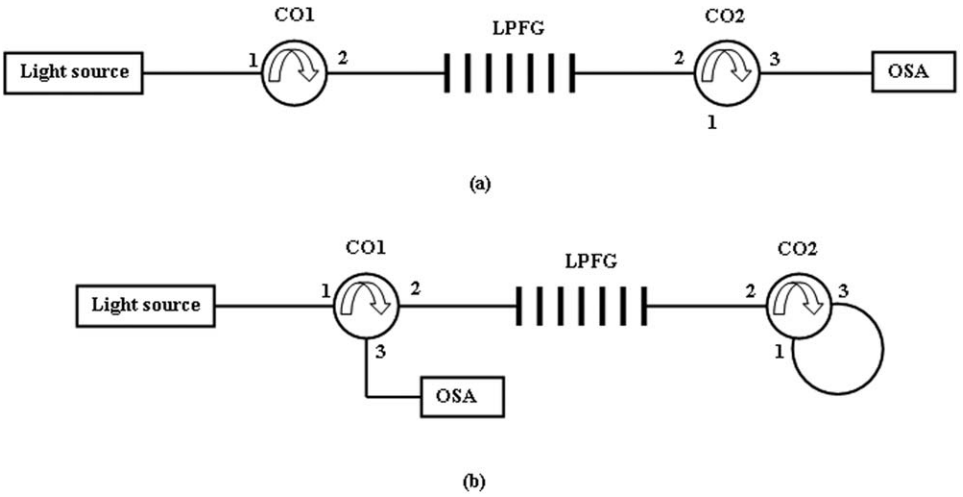

Figure 1 (a) Single-pass configuration and (b) Double-pass configuration

The pristine avidin-immobilized LPFG sensor was then connected using single-pass and double-pass configurations. Two polarization independent circulators were used to achieve the double-pass configuration as shown in Figure 1. Results of avidin–biotin interaction were obtained when the pristine avidin-immobilized LPFG was submerged into PBS with pH 7.5 and containing 10 mM of sulfo-NHS-SS-biotin were recorded every minute for both single-pass and double-pass configurations.

3. RESULTS AND DISCUSSION

Figure 2(a) compares the transmission attenuation of the resonance wavelength for a bare arc-induced LPFG, that is, for both single-pass and double-pass configurations. It is visible that the double-pass configuration has higher transmission attenuation compared to the single-pass configuration. The double-pass action allowed the optical signal to pass through the grating twice the length of the single-pass configuration, thus allowing higher attenuation of the resonance wavelength. The transmission attenuation of the resonance wavelength of the double-pass configuration is about 20 dBm as compared to the single pass which was about 10 dBm. The higher attenuation for the double-pass configuration is due to the higher coupling strength which is directly influenced by the grating length. The transmittance of the LPFGs varies following the term $\cos^2(\kappa L)$ when the phase-matching condition is satisfied at $\Delta\beta = 0$, where κ is the coupling coefficient and L the grating length [16].

To test the sensitivity of the proposed double-pass configuration, the avidin-immobilized LPFG was used to monitor the avidin–biotin interaction. The transmission spectra of the avidin-immobilized LPFG in PBS (as reference) and in PBS containing biotin for both double-pass and single-pass configuration are shown in Figures 2(b) and 2(c), respectively. From Figures 2(b) and 2(c), it was observed that there was slight blue shifting of the LPFG resonance wavelength during the avidin–biotin interaction, whereas the transmission attenuation of the LPFG resonance wavelength increased as compared to the reference spectra for both configurations. The changes were more obvious for the double-pass configuration as compared to the single-pass.

Figure 3 shows the avidin-immobilized LPFG resonance wavelength during the avidin–biotin interaction in both single-pass and double-pass configurations over a period of 60 min. There were not any significant changes in the resonance wavelength of the notch over time for both single-pass and double-pass, although the double-pass showed larger variation as compared to the single-pass. This is a strong indication that there was no significant change in the optical thickness of the avidin-biotin overlay forming on the grating surface which influences the effective index of the cladding. This is supported by $\lambda_i = (n_{\text{core}}(\lambda_i) - n^i_{\text{clad}}(\lambda_i))\ \Lambda$, where λ_i is the resonance wavelength, $n_{\text{core}}(\lambda_i)$ is the effective index of the core mode, $n^i_{\text{clad}}(\lambda_i)$ is the effective index of the ith cladding mode and Λ is the grating period. With the formation of the avidin-biotin overlay, the effective refractive index of cladding increases, which makes the effective refractive index difference of the core and cladding to decrease thus resulting in the blue shift of the resonance wavelength. There were no significant changes of the resonance wavelength over time as the avidin–biotin interaction forms a monoloyer that do not affect the overall effective index of the cladding.

Figure 4 shows the normalized transmission attenuation of the LPFG resonance wavelength during the avidin–biotin interaction of both single-pass and double-pass configurations over a period of 60 min. The change of transmission attenuation was more significant in double-pass configuration as compared to the single-pass configuration. Single-pass configuration has a variation of the normalized transmission attenuation of about 0.336 a.u., whereas the double-pass configuration has a variation of the normalized transmission attenuation of about 0.666 a.u. The normalized transmission attenuation was calculated relative to the reference spectra of respective configurations and by first converting the attenuation from dBm to μW. The gradient of the slope (beyond 30 min) of the single-pass configuration was measured to be around −0.0097 (a.u./mins.) whereas it was −0.0160 (a.u./mins.) for the double-pass configuration. This indicates that the double-pass configuration has a sensitivity of almost double as compared to the single-pass configuration, that is, in terms of the transmission attenuation of the resonance wavelength. The increase in the transmission attenuation of the resonance wavelength, for double-pass and single-pass configurations is due to the increase in the overlap of the core and cladding modes induced by the overlay film formed during the avidin–biotin interaction. However, for the double-pass configuration the attenuation showed better sensitivity to the interaction

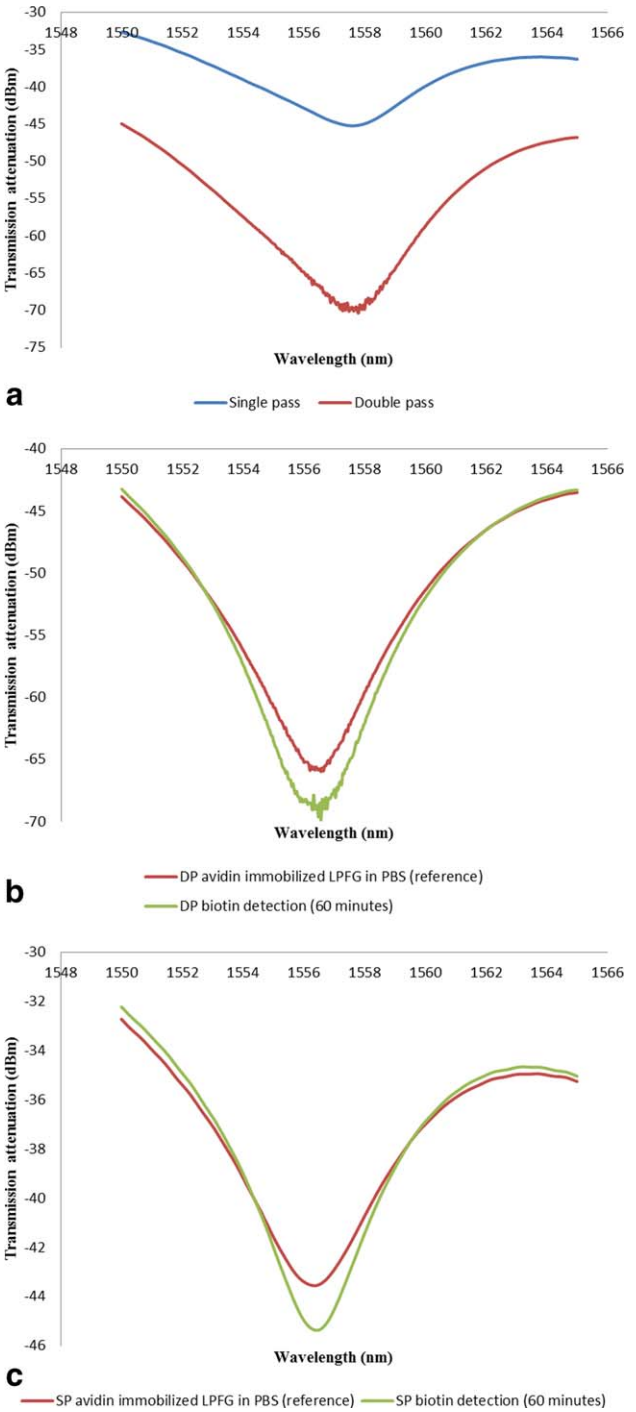

Figure 2 (a) Transmission of bare LPFG for single-pass and double-pass configuration, (b) Transmission of avidin-immobilized LPFG in PBS (reference) and avidin–biotin interaction (60 min) for the double-pass configuration, and (c) Transmission of avidin-immobilized LPFG in PBS (reference) and avidin–biotin interaction (60 min) for the single-pass configuration. [Color figure can be viewed in the online issue, which is available at wileyonlinelibrary.com]

between avidin and biotin which may be attributed to the transmission characteristics of the LPFG which is influenced by the transmittance factor $\cos^2(\kappa L)$ [16].

4. CONCLUSION

Results showed that the double-pass configuration of the avidin-immobilized LPFG sensor was sensitive to the change of the

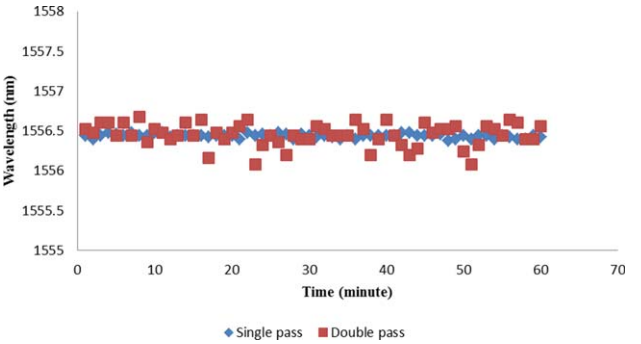

Figure 3 Resonance wavelength (nm) versus time (minutes) during monitoring of the avidin–biotin interaction for both single- and double-pass. [Color figure can be viewed in the online issue, which is available at wileyonlinelibrary.com]

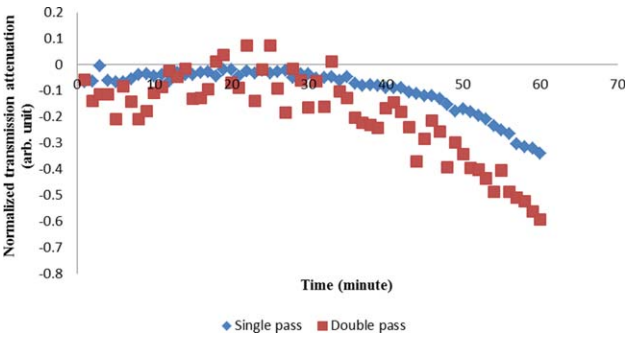

Figure 4 Normalized transmission attenuation of the LPFG resonance wavelength versus time during monitoring of the avidin–biotin interaction. [Color figure can be viewed in the online issue, which is available at wileyonlinelibrary.com]

transmission attenuation compared to the single-pass configuration during the avidin–biotin interaction. There was not much change in the wavelength shift for both double-pass and single-pass configurations over 60 min of exposure, although the double-pass showed larger variation. The high affinity of the biotin-avidin systems makes it easier to confirm that the change in the transmission attenuation is due to the biotin-avidin interaction instead of interactions of avidin with other foreign matter. The result of the experiments conducted proves that the double-pass arc-induced LPFG configuration is a promising method to improve the sensitivity of the optical sensor especially for applications which requires long term monitoring of chemical or biological reactions which does not involve significant change in the refractive index.

ACKNOWLEDGMENT

The project is sponsored under the Fundamental Research Grant Scheme (FRGS), Ministry of Higher Education, Malaysia (FRGS/2/2101/ SG/UTAR/01/1).

REFERENCES

1. A.M. Vengsarkar, P.J. Lernaire, J.B. Judkins, V. Bhatia, T. Erdogan, and J.E. Sipe, Long-period fiber gratings as band-rejection filters, J Lightwave Technol 14(1996), 58–64.
2. M. Smietana, W.J. Bock, P. Mikulic, and J. Chen, Increasing sensitivity of arc-induced long-period gratings—pushing the fabrication technique toward its limits, Meas Sci Technol 22 (2011), 015201.

3. W.J. Bock, J. Chen, P. Mikulic, and T. Eftimov, A novel fiber-optic tapered long-period grating sensor for pressure monitoring, IEEE Trans Instrum Meas 56 (2007), 1176–1180.
4. X. Shu, L. Zhang, and I. Bennion, Sensitivity characteristics of long-period fiber gratings, J Lightwave Technol 20 (2002), 255–266.
5. M. Mysliwiec, J. Grochowski, K. Krogulski, P. Mikulic, W.J. Bock, and M. Smietana, Effect of wet etching of arc-induced long-period gratings on their refractive index sensitivity, Acta Physica Polonica A 124 (2013), 521–524.
6. S. Chaubey, S. Kher, J. Kishore, and S.M. Oak, CO2 laser-inscribed low-cost, shortest-period long-period fibre grating in B-Ge co-doped fibre for high-sensitivity strain measurement, Pramana 8 (2014), 373–377.
7. S.F. Cheng and L.K. Chau, Colloidal gold-modified optical fiber for chemical and biochemical sensing, Anal Chem 75 (2003), 16–21.
8. S. Ik-Bu and S. Jae-Won, Gain flattened and improved double-pass two-stage EDFA using microbending long-period fiber gratings, Opt Commun 236 (2004), 141–144.
9. S.W. Harun and H. Ahmad, Low noise double pass L-band erbium-doped fiber amplifier, Opt Laser Technol 35 (2004), 245–248.
10. T.-C. Liang and S. Hsu, The L-band EDFA of high clamped gain and low noise figure implemented using fiber Bragg grating and double-pass method, Opt Commun 281 (2008), 1134–1139.
11. R.P. Haugland and M.K. Bhalgat, Preparation of Avidin conjugates, In: R.J. McMahon, (Ed.), Avidin-Biotin interactions: Methods and applications, Vol. 418, 2008, pp. 1–12.
12. R.P. Haugland and W.W. You, Coupling of Antibodies with Biotin, In: R.J. McMahon, (Ed.), Avidin-Biotin Interactions: Methods and Applications, Vol. 418, 2008, pp. 25–34.
13. F.J. Hernandez, S.K. Dondapati, V.C. Ozalp, A. Pinto, C.K. O'Sullivan, T.A. Klar, and I. Katakis, Label free optical sensor for Avidin based on single gold nanoparticles functionalized woth aptamers, J Biophoton 2 (2009), 227–231.
14. S. Krizkova, V. Hrdinova, V. Adam, E.P.J. Burgess, K.J. Kramer, M. Masarik, and R. Kizek, Chip-Based CE for Avidin determination in transgenic tobacco and its comparison with square-wave voltammetry and standard gel electrophoresis, Chromatographia 67 (2008), Supplement 75–81.
15. Y. Shao, S. Xu, X. Zheng, Y. Wang, and W. Wu, Optical fiber LSPR biosensor prepared by gold nanoparticle assembly on polyelectrolyte multilayer, Sensors 10 (2010), 3585–3596.
16. H. Young-Geun, Dependence of the refractive index of a coating on a long-period fiber grating on the initial coupling strength, J Korean Phys Soc 55 (2009), 2621–2624.

IMPLEMENTATION OF ELECTRONIC BEAM STEERING SYSTEM USING LOOK-UP TABLE CALIBRATION METHOD

Sung-hoon Jang,[1] Jong-phil Kim,[2] Seon-joo Kim,[1] and Chang-yul Cheon[3]
[1] Radar Division, Agency for Defense Development, Daejeon, Korea; Corresponding author: jangsh@add.re.kr
[2] ISR Center, LIG NEX1, Yongin, Korea
[3] Department of Electrical and Computer Engineering, University of Seoul, Seoul, Korea

Received 25 April 2014

ABSTRACT: *This article presents a design and implementation of the electronically beam steering system for active electronically scanning array (AESA) radar. This beam steering system used look-up table (LUT) calibration method to calibrate an amplitude and phase errors of each T/R Modules. LUT contains the T/R Module characterization data and the antenna correction data. Performance of this beam steering system was verified with the X-band AESA radar demonstrator which has 1024 radiating elements and 504 T/R Modules. Beam steering angle is ±60° in each azimuth and elevation. Beam steering time is 3 μs using the precalculation method of the next steering position.* © 2014 Wiley Periodicals, Inc. Microwave Opt Technol Lett 56:2769–2773, 2014; View this article online at wileyonlinelibrary.com. DOI 10.1002/mop.28700

Key words: *airborne radar; active electronically scanning array; beam steering system; phase gradient; look-up table*

1. INTRODUCTION

Active electronically scanning array (AESA) antenna has several advantages compared to mechanical scanning antenna. Instantaneous beam steering to the desired position is possible with AESA antenna. AESA antenna front face can be fixed, so no mechanical motor is needed to scanning the beam.

In general, AESA radar has several hundreds or thousands number of transmit/receive modules (TRMs). Each TRMs have to be precisely controlled to steer the beam to the desired position. In real operation, TRMs contains phase and amplitude error with frequency, temperature, and beam steering angle. Also, RF path difference and mechanical fabrication tolerance can make additional errors to each TRMs channels.

Research on the beam steering system design for phased array antenna has been published in [1,2], and its practical implementation was presented in [3]. However, there is no detailed description how to calibrate the phase and amplitude errors of TRMs in real radar operation.

In this article, we proposed the look-up table (LUT) calibration method to compensate the phase and amplitude errors in AESA antenna. The proposed LUT contains antenna correction data and T/R Module characterization data. Section 2 presents the design results of the beam steering system for AESA antenna. LUT calibration process is described in Section 3. Section 4 describes the measurement results of the proposed beam steering system.

2. DESIGN

The configuration of an AESA antenna is shown in Figure 1. This antenna is formed by a triangular lattice array of $m \times n$ radiation elements. Triangular lattice structure can reduce the array element number about 10% comparing with the rectangular lattice array. The numbers of radiating elements are m and n in each x and y axis. The interelement spacing in the two

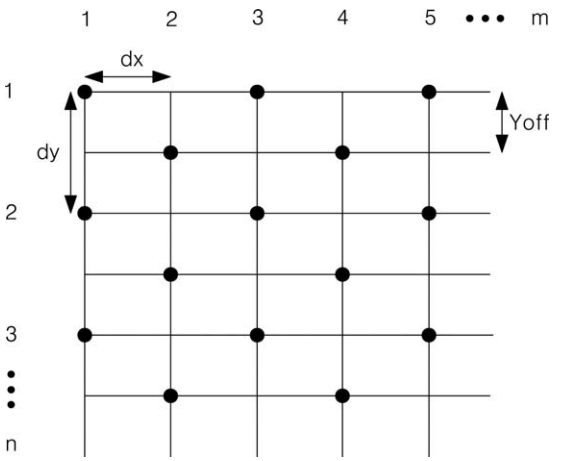

Figure 1 Triangular lattice structure of radiating elements for phased array